1 Supplements

1.1 Detailed model description

The reactions in the reactive transport model describe organic matter degradation coupled to different electron acceptors. Reactions are divided in primary redox reactions and other biogeochemical reactions (Table S.6). The succession of oxidants during organic matter degradation (Froelich et al., 1979) is described by means of Monod kinetics (Table S.2; Boudreau (1997)). This means that the oxidants with the highest metabolic free energy yield are preferentially used until they become limiting and the oxidant with the next highest energy yield is used (Berg et al., 2003; Boudreau, 1996a; Wang and Van Cappellen, 1996). Respiratory reactions occur where O_2, NO_3^-, $Mn(OH)_2$, $Fe(OH)_3$ and SO_4^{2-} serve as electron acceptors and finally organic matter is subject to methanogenesis (Reed et al. (2011a, b); Rooze et al. (2016); Table S.2). Organic matter includes carbon (C), nitrogen (N) and P in a C:N:P ratio of 106:16:0.35. In the model, oxidation of CH_4 is possible with O_2, $Mn(OH)_2$, $Fe(OH)_3$ and SO_4^{2-}. Dissolved inorganic carbon in the model is calculated as the sum of the carbon in CO_2 and HCO_3^{2-}, which is produced or consumed by modeled reactions (Table S.6).

The generic mass conservation equations for solids and solutes are described by Eq. 1 and 2;

$$(1-\phi)\frac{\partial C_s}{\partial t} = -(1-\phi)v\frac{\partial C_s}{\partial z} + \sum R_s \tag{1}$$

$$\phi\frac{\partial C_{aq}}{\partial t} = \phi D'\frac{\partial^2 C_{aq}}{\partial z^2} - \phi u\frac{\partial C_{aq}}{\partial z} + \sum R_{aq} \tag{2}$$

$$D' = \frac{D_m}{1 - ln\phi^2} \tag{3}$$

where C_s is the concentration of solid species ($\mathrm{mol\ L^{-1}}$), C_{aq} is the concentration of dissolved species ($\mathrm{mol\ L^{-1}}$), t is time (yr), ϕ is the sediment porosity, v and u are the advective velocities of solid and dissolved species ($\mathrm{cm\ yr^{-1}}$), respectively. Variables v and u were described by a depth-dependent function to account for changes in porosity (Meysman et al., 2005). Distance from the sediment-water interface is z (cm), D' the diffusion coefficient of dissolved species ($\mathrm{cm^2\ yr^{-1}}$), corrected for tortuosity in the porous medium ((Boudreau, 1996b), Eq. 3). $\sum R_s$ and $\sum R_{aq}$ are the net reaction rates from the chemical reaction (Table S.2) for solid and dissolved species.

Porosity (ϕ) is described by Eq. 4 to account for sediment compaction (Meysman et al., 2005; Reed et al., 2011b),

$$\phi(x) = \phi_\infty + (\phi_0 - \phi_\infty)e^{-\frac{x}{y}} \tag{4}$$

where ϕ_0 is the porosity at the sediment-water interface, ϕ_∞ is the porosity at depth and y is the porosity attenuation factor/e-folding distance (Fig. S.3A, Table S.3). The model code was written in R with the use of the marelac geochemical dataset package (Soetaert et al., 2010). To calculate the transport in porous media, the R package Reactran was used (Soetaert and Meysman, 2012). The set of ordinary differential equations was solved numerically with the Lsode integrator algorithm (Petzold, 1983).

Zero gradient boundary conditions were applied to the base of the model domain for all chemical species. To avoid influence of the boundary conditions at the base of the model domain results, the total depth of the model was set to 90 cm (divided into 900 grid cells of 0.1 cm).

Reaction parameters were mostly taken from literature or obtained within existing parameter ranges (Table S.7). If these were not available, or no fit to the data could be obtained with existing ranges, parameters were constrained by fitting the model to the measured data.

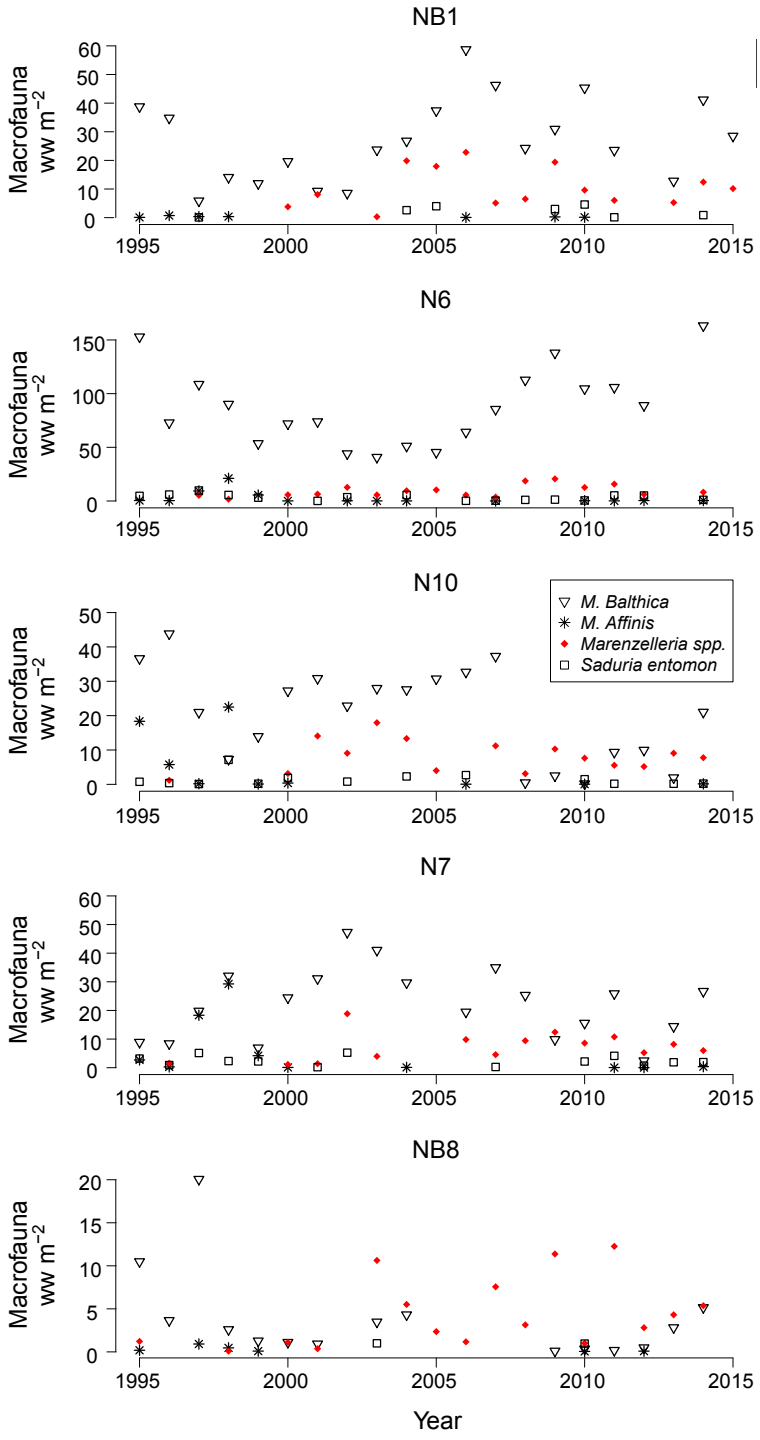

Figure S.1. Wet weight of macrofauna (ww m^{-2}; in grams) at sites NB1, N6, N10, N7 and NB8 in the Öre Estuary from 1995-2015 (www.SMHI.se).

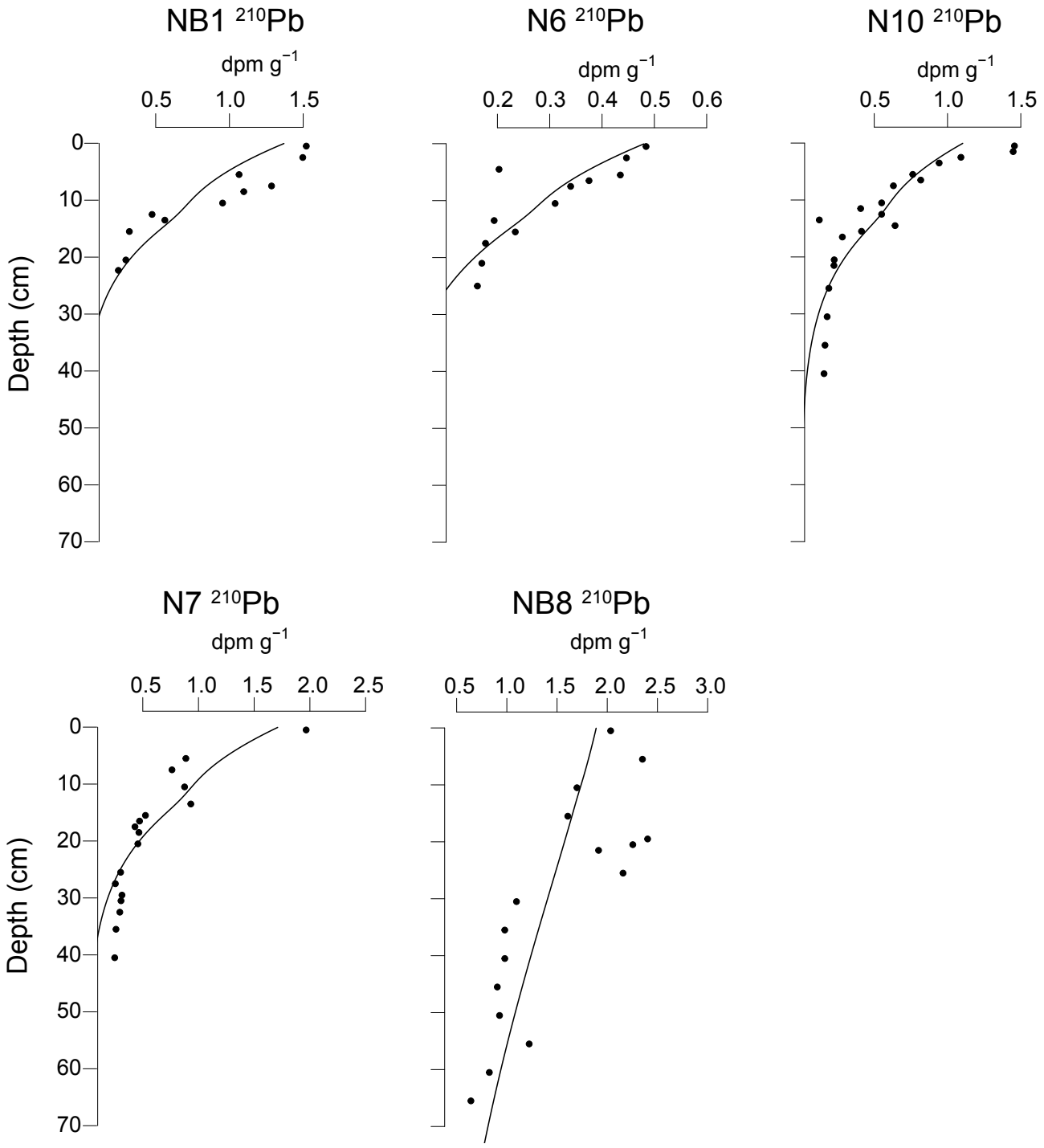

Figure S.2. Solid phase depth profiles of ^{210}Pb at sites NB1, N6, N10, N7 and NB8 and model fits (black lines). Sites NB1, N6, N10 and N7 were sampled in April 2015. Site NB8 was sampled in August 2015.

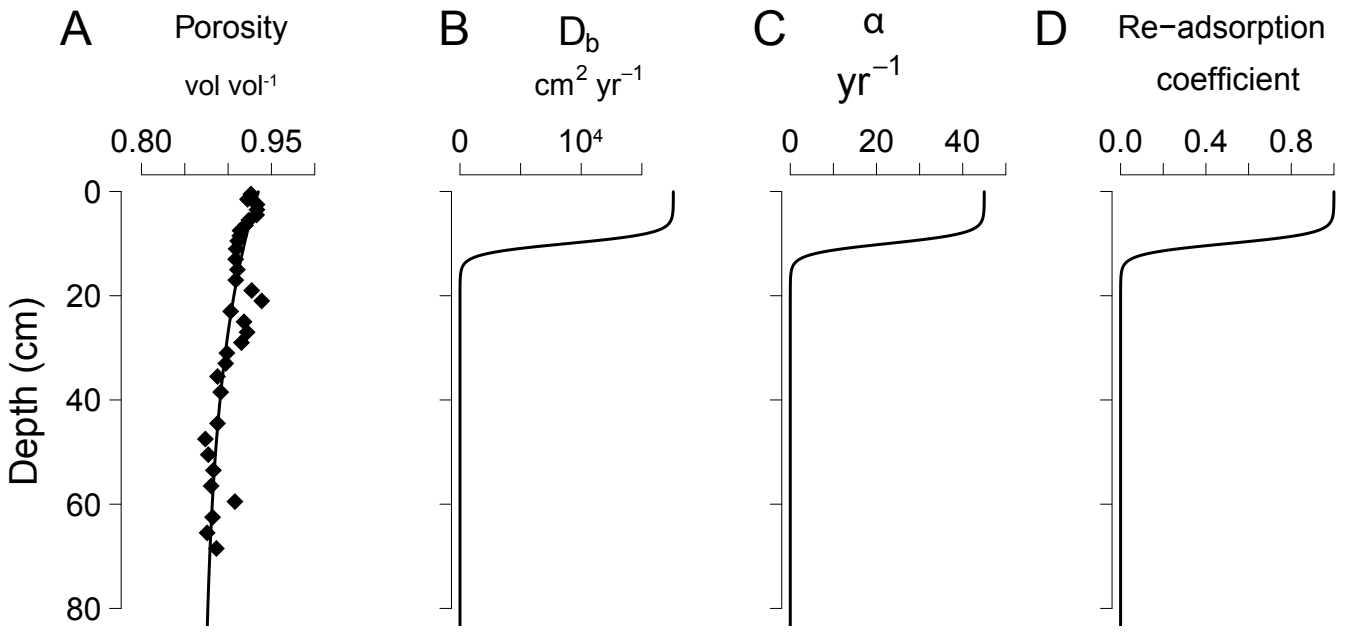

Figure S.3. Depth profiles used in the model A: Measured porosity ($\mathrm{vol\ vol^{-1}}$) for April 2015 (black circles) and fitted porosity (black line); B: bioturbation coefficient (D_b; $\mathrm{cm\ yr^{-1}}$); C: bioirrigation coefficient (α; $\mathrm{yr^{-1}}$); D: Re-adsorption coefficient for HPO_4^{2-}.

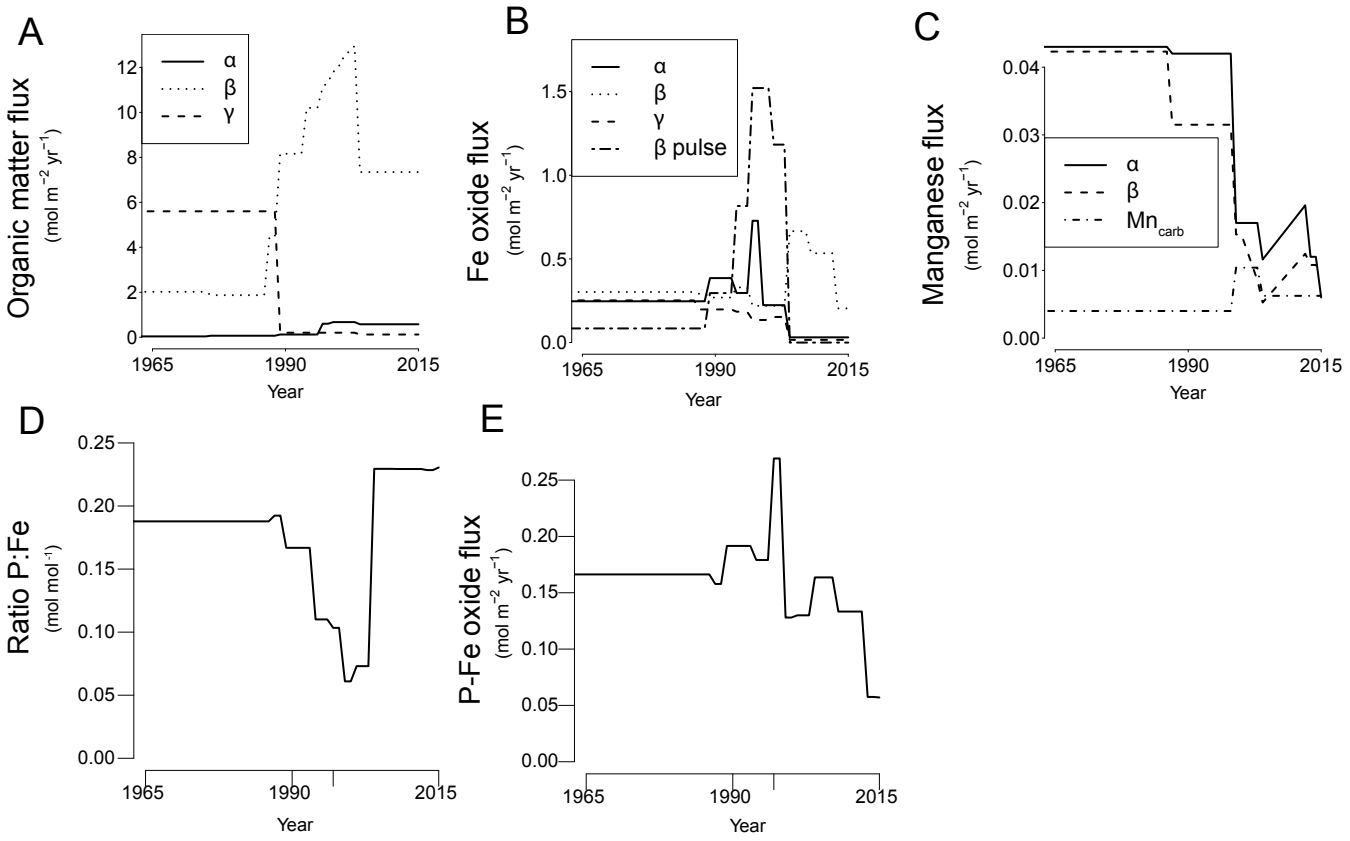

Figure S.4. Transient scenarios used in the reactive transport model between 1965 and 2015; A: different phases of organic matter; B different phases of Fe oxides; C: different phases of manganese; D: average P:Fe ratio of all Fe oxide fractions combined, E: total P input bound to Fe oxides. The various types of organic matter, Fe oxides and Mn oxides are indicated as α (highly reactive), β (less reactive) and γ (refractory).

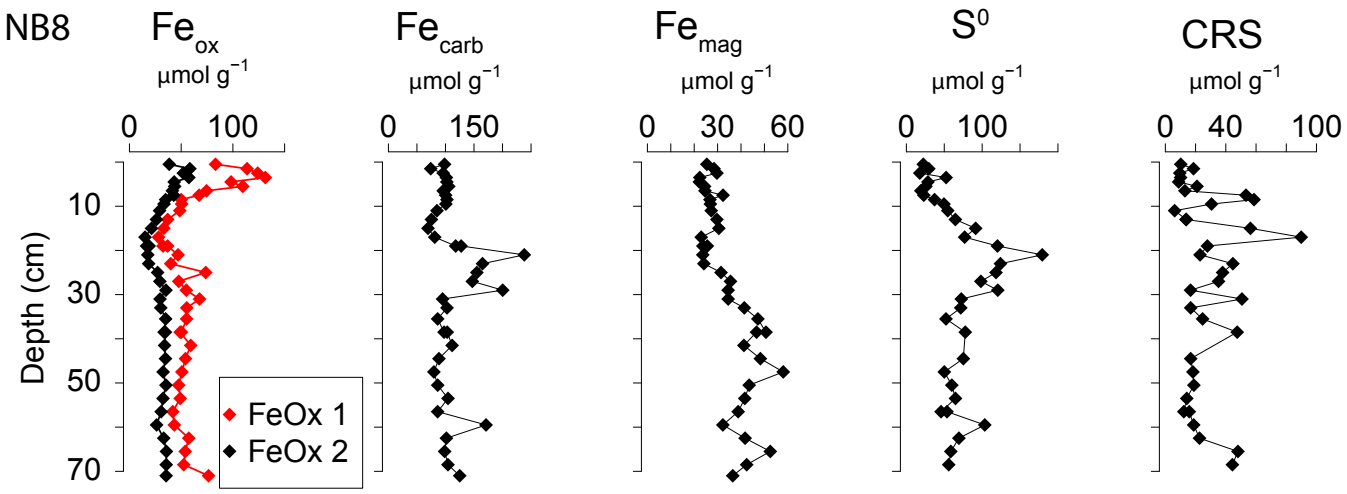

Figure S.5. Solid phase depth profiles of the easily reducible Fe oxides (Fe_{ox1}) and reducible (crystalline) Fe oxides (Fe_{ox2}) including vivianite, Fe carbonates (Fe_{carb}), magnetite (Fe_{mag}), elemental S (S^0) and S in pyrite (CRS) for site NB8 in April 2015.

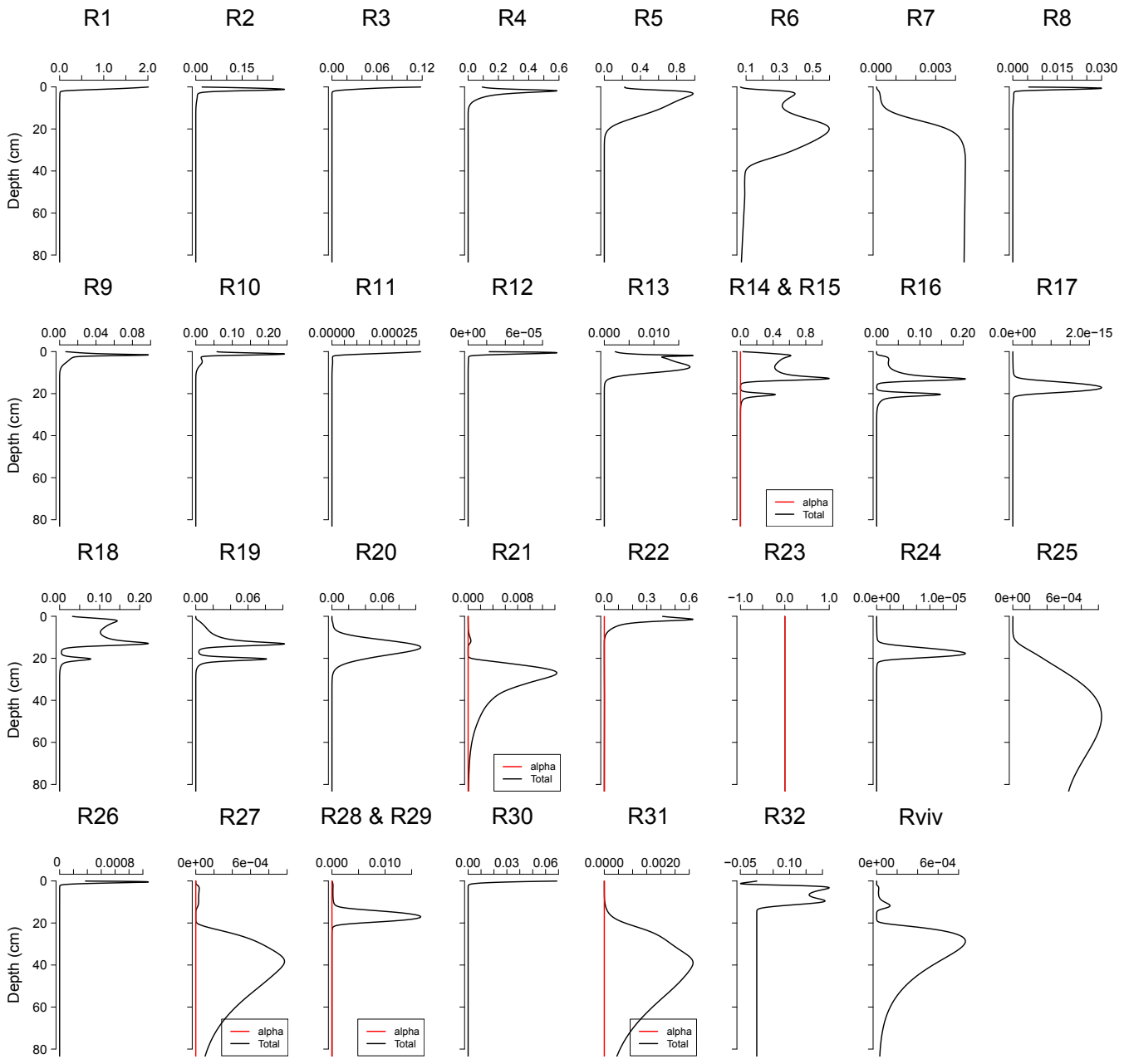

Figure S.6. Depth profiles of reaction rates calculated for the baseline scenario in 2015. Rates are in $\mathrm{mol\ m^{-3}\ yr^{-1}}$. Reactions are described in Table S.6.

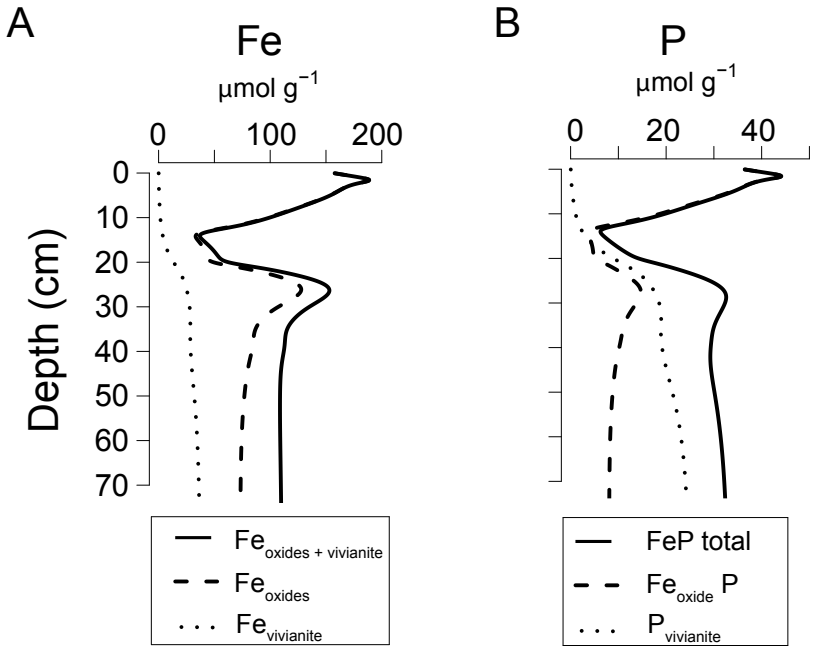

Figure S.7. Solid phase depth profiles of A: Fe bound to Fe oxides and vivianite; B: P bound to Fe oxides and vivianite.

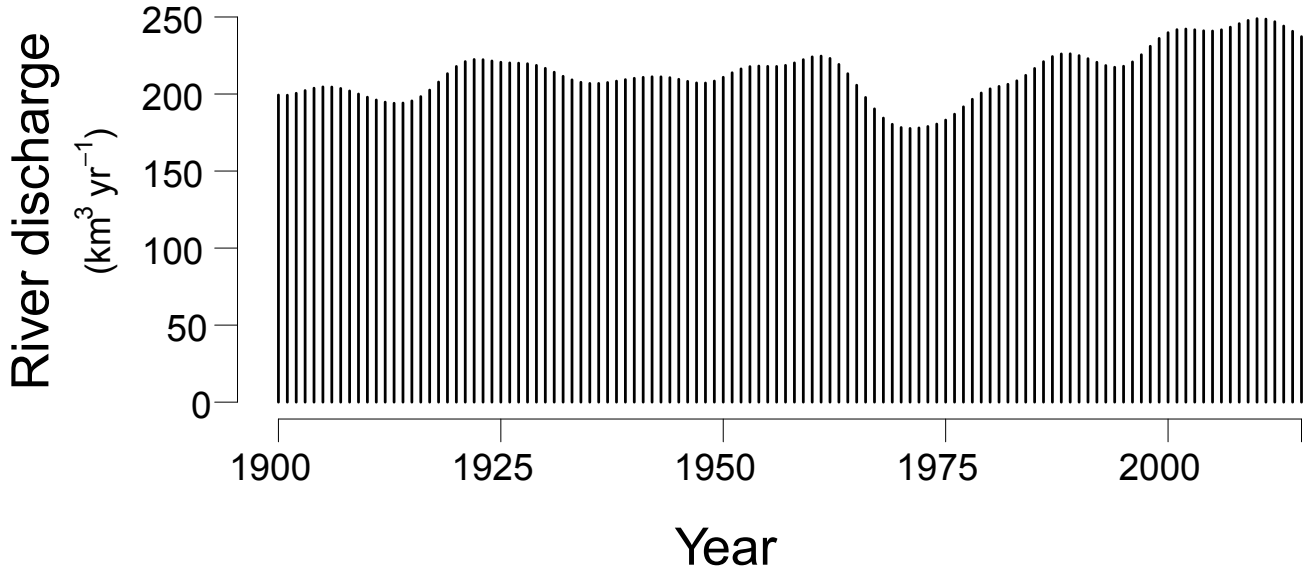

Figure S.8. Averaged summer river discharge for 86 Swedish rivers from 1900-2015 (www.SMHI.se).

Table S.1. Chemical species included in the model.

Species	**Notation**
Solid	
Organic matter[a]	$OM^{\alpha,\beta,\gamma}$
Iron oxide[a]	$Fe(OH)_3{}^{\alpha,\beta}$
Elemental sulfur	S^0
Iron monosulfide	FeS
Pyrite	FeS_2
Iron-bound Phosphorus	$Fe(OH)_3P$
Vivianite	$Fe_3(PO_4)_2$
Siderite	$FeCO_3$
Organic phosphorus	P_{org}
Authigenic (Ca) phosphorus	CaP
Detrital phosphorus	DetrP
Manganese oxide[b]	$Mn(OH)_2{}^{\alpha,\beta}$
Manganese carbonate	$MnCO_3$
Solute	
Chloride	Cl^-
Oxygen	O_2
Nitrate	$NO_3{}^-$
Sulfate	$SO_4{}^{2-}$
Methane	CH_4
Iron	Fe^{2+}
Ammonium[c]	$\sum NH_4{}^+$
Hydrogen sulfide[c]	$\sum H_2S$
Phosphate[c]	$\sum HPO_4{}^{2-}$
Dissolved Inorganic Carbon	DIC
Manganese	Mn^{2+}

[a] chemical species consist of 3 types: reactive (α), less reactive (β) and refractory (γ). Fe oxide$^{\beta(pulse)}$ and Fe oxide$^{\beta(max)}$ are not specifically named because they have the same characteristics as Fe oxide$^{\beta}$.

[b] chemical species consist of two types: reactive (α) and less reactive (β).

[c] $\sum$ denotes that all species of an acid are included.

Table S.2. Reaction pathways and stoichiometries implemented in the model.

Primary redox reactions	
$OM^{\alpha,\beta} + aO_2 \rightarrow aCO_2 + bNH_4^+ + cH_3PO_4 + aH_2O$	R1
$OM^{\alpha,\beta} + 0.8aNO_3^- + 0.8aH^+ \rightarrow aCO_2 + bNH_4^+ + cH_3PO_4 + 0.4aN_2 + 1.4a\ H_2O$	R2
$OM^{\alpha,\beta} + 2aMn(OH)_2{}^{\alpha} + 2aH^+ \rightarrow 2\ Mn^{2+} + aCO_2 + cH_3PO_4 + 2aH_2O$	R3
$OM^{\alpha,\beta} + 4a\ Fe(OH)_3{}^{\alpha} + 4a\chi^{\alpha}Fe_{ox}P + 12aH^+ \rightarrow aCO_2 + bNH_4^+ + (c+4a\chi^{\alpha})H_3PO_4 + 13aH_2O + 4aFe_2^+$	R4
$OM^{\alpha,\beta} + 0.5a\ SO_4^{2-} + aH^+ \rightarrow aCO_2 + bNH_4^+ + cH_3PO_4 + 0.5aH_2S + aH_2O$	R5
$OM^{\alpha,\beta} \rightarrow 0.5aCO_2 + bNH_4^+ + cH_3PO_4 + 0.5aCH_4$	R6
$CO_2 + 4H_2 \rightarrow CH_4 + 2H_2O$	R7
Secondary and other reactions	
$2O_2 + NH_4^+ + 2HCO_3^- \rightarrow NO_3^- + 2CO_2 + 3H_2O$	R8
$O_2 + 4Fe^{2+} + 8HCO_3^- + 2H_2O + 4\chi^{\alpha}H_2PO_4^- \rightarrow 4\ Fe(OH)_3{}^{\alpha} + 4\chi^{\alpha}\ Fe_{ox}P + 8CO_2$	R9
$2O_2 + FeS \rightarrow SO_4^{2-} + Fe^{2+}$	R10
$7O_2 + 2FeS_2 + 2H_2O \rightarrow 4SO_4^{2-} + 2Fe^{2+} + 4H^+$	R11
$2O_2 + H_2S + 2HCO_3^- \rightarrow SO_4^{2-} + 2CO_2 + 2H_2O$	R12
$2O_2 + CH_4 \rightarrow CO_2 + 2H_2O$	R13
$2Fe(OH)_3{}^{\alpha} + 2\chi^{\alpha}Fe_{ox}P + H_2S + 4CO_2 \rightarrow 2Fe^{2+} + 2\chi^{\alpha}H_2PO_4^- + S^0 + 4HCO_3^- + 2H_2O$	R14
$2Fe(OH)_3{}^{\beta,\beta(max),\beta(pulse)} + 2\chi^{\alpha}Fe_{ox}P + H_2S + 4CO_2 \rightarrow 2Fe^{2+} + 2\chi^{\alpha}H_2PO_4^- + S^0 + 4HCO_3^- + 2H_2O$	R15
$Fe^{2+} + H_2S \rightarrow FeS + 2H^+$	R16
$FeS + H_2S \rightarrow FeS_2 + H_2$	R17
$4S_0 + 4H_2O \rightarrow 3H_2S + SO_4^{2-} + 2H^+$	R18
$FeS + S^0 \rightarrow FeS_2$	R19
$SO_4^{2-} + CH_4 + CO_2 \rightarrow 2HCO_3^- + H_2S$	R20
$CH_4 + 8Fe(OH)_3{}^{\alpha,\beta,\beta(max),\beta(pulse)} + 8\chi^{\alpha,\beta}\ Fe_{ox}P + 15H^+ \rightarrow HCO_3^- + 8Fe^{2+} + 8\chi^{\alpha,\beta}H_2PO_4^- + 21H_2O$	R21
$Fe(OH)_3{}^{\alpha} + (\chi^{\alpha} - \chi^{\beta})Fe_{ox}P \rightarrow Fe(OH)_3{}^{\beta} + (\chi^{\alpha} - \chi^{\beta})H_2PO_4^-$	R22
$Fe^{2+} + CO_3^{2-} \rightarrow FeCO_3$	R23
$Fe(PO_4)_2 + 3H_2S \rightarrow 2FeS + 2HPO_4^{2-} + 4H^+$	R24
$Mn^{2+} + HCO_3^- + OH^- \rightarrow MnCO_3 + H_2O$	R25
$2Mn^{2+} + 2O_2 + 4H^+ \rightarrow 2Mn(OH)_2{}^{\alpha}$	R26
$Mn(OH)_2{}^{\alpha,\beta} + 2H_3PO_4 + 2Fe^{2+} \rightarrow Mn^{2+} + 2\chi^{\alpha}Fe_{ox}P$	R27
$Mn(OH)_2{}^{\alpha} + H_2S \rightarrow Mn^{2+} + S_0 + 2H_2O$	R28
$Mn(OH)_2{}^{\beta} + H_2S \rightarrow Mn^{2+} + S_0 + 2H_2O$	R29
$Mn(OH)_2{}^{\alpha} \rightarrow Mn(OH)_2{}^{\beta}$	R30
$4\ Mn(OH)_2{}^{\alpha,\beta} + CH_4 + 7H^+ \rightarrow 4Mn^{2+} + HCO_3^- + 5H_2O$	R31
$Fe(OH)_3{}^{\beta,\beta(pulse)} + (\chi^{\beta(max)} - \chi^{\beta,\beta(pulse)})HPO_4^{2-} \rightarrow Fe(OH)_3{}^{\beta(max)}$	R32

Organic matter is of the form $((CH_2O)_a(NH_4^+)_b(H_3PO_4)_c$, where a=1, b= 1/16 and c = 300/1. α, β, & γ describe different fractions (i.e. highly reactive, less reactive and refractory). $\chi^{\alpha,\beta,\gamma}$ describes the different P:Fe ratios of $Fe(OH)_3^{\alpha,\beta,\gamma}$. Reactions for different $Fe(OH)_3{}^{\beta}$ fractions (β, $\beta(max)$ and $\beta(pulse)$ are the same and are therefore combined as $Fe(OH)_3{}^{\beta}$).

Table S.3. Environmental parameters used in the model.

Description	Symbol	Value or expression	unit	source
Porosity at the Surface	ϕ_0	0.935	vol vol^{-1}	a
Porosity at depth	ϕ_∞	0.87	vol vol^{-1}	a
Porosity e-folding distance	γ	35	cm	b
Sediment density	ρ	2.65	g cm^{-3}	c
Temperature	T	2.77	°C	a
Salinity	S	5.05		a
Advective velocity of solids at depth	v_∞	$\frac{F_{sed}}{\rho(1-\phi_\infty)}$		–
Bioturbation coefficient at sediment-water interface	D_b	1.76	cm^2 yr^{-1}	b
Bioirrigation coefficient at sediment-water interface	α	45*10^4	yr^{-1}	b
Mixed layer depth	ς	11	cm	b
C:N ratio of organic matter	C/N	6.625	mol mol^{-1}	d
C:P ratio of organic matter	C/P	300	mol mol^{-1}	b
P:$Fe(OH)_3{}^{\alpha}$	χ^{α}	0.28	mol mol^{-1}	b
P:$Fe(OH)_3{}^{\beta}$	χ^{β}	0.23	mol mol^{-1}	b
P:$Fe(OH)_3{}^{\gamma}$	χ^{γ}	0.11	mol mol^{-1}	b
P:$Fe(OH)_3{}^{\beta(max)}$	$\chi^{\beta(max)}$	0.28	mol mol^{-1}	b
P:$Fe(OH)_3{}^{\beta(pulse)}$	$\chi^{\beta(pulse)}$	0	mol mol^{-1}	b

Sources: (a) Measured; (b) Model constrained; (c) Reed et al. (2011b); (d) Redfield (1958).

Table S.4. Boundary conditions of solids and solutes at the sediment-water interface in the model. Time dependent fluxes of $OM^{\alpha,\beta,\gamma}$, $Fe(OH)_3{}^{\alpha,\beta,\gamma}$, $Mn(OH)_2{}^{\alpha,\beta}$, Mn carbonates and sedimentation rate at the sediment-water interface are shown in figure 3. For all chemical species a zero-gradient boundary condition was specified at the bottom of the model domain.

Solids	Flux at sediment water interface	Unit
F FeS	0	mol m^{-2} yr^{-1}
F FeS_2	0	mol m^{-2} yr^{-1}
F S0	0	mol m^{-2} yr^{-1}
F $FeCO_3$	0.27	mol m^{-2} yr^{-1}
F Vivianite	0	mol m^{-2} yr^{-1}
F Detr. P	0.034	mol m^{-2} yr^{-1}
F Auth. P	0.03	mol m^{-2} yr^{-1}
Solutes	**BW concentration**	**Unit**
C O_2	0.091	mol m^{-3}
C $NO_3{}^-$	0	mol m^{-3}
C $SO_4{}^{2-}$	4.05	mol m^{-3}
C Fe^{2+}	0	mol m^{-3}
C Mn^{2+}	0	mol m^{-3}
C H_2S	0	mol m^{-3}
C $NH_4{}^+$	0	mol m^{-3}
C $HPO_4{}^{2-}$	0.21	mol m^{-3}
C DIC	1.5	mol m^{-3}

Table S.5. Analyses of vivianite crystals from below the SMTZ at site NB8 with electron microprobe-EDS. Vivianite crystals were collected from 3 different depths. The average value and standard deviation for each element was caulculated from 7 EDS point analyses.

Element	**mol %**
O	37.8 ± 3.4
Na	0.4 ± 0.2
Mg	0.8 ± 0.6
Al	6.3 ± 6.2
Si	2.6 ± 1.5
P	13.5 ± 5.4
Ca	0.3 ± 0.2
Mn	6.9 ± 2.3
Fe	31.4 ± 6.3
	mol mol^{-1}
Fe/P	3.3 ± 2.0
Fe/Mn	4.7 ± 0.8
(Fe+Mn)/P	4.1 ± 2.5
Mn/P	0.8 ± 0.5
(Fe+Mn+Mg)/P	4.3 ± 2.5

Table S.6. Reaction equations implemented in the model.

Primary redox reaction equations	
$R1 = k_{\alpha,\beta} OM^{\alpha,\beta} \left(\frac{[\mathrm{O_2}]}{K_{m,\mathrm{O_2}} + [\mathrm{O_2}]} \right)$	E1
$R2 = k_{\alpha,\beta} OM^{\alpha,\beta} \left(\frac{[\mathrm{NO_3}^-]}{K_{m,\mathrm{NO_3}^-} + [\mathrm{NO_3}^-]} \right) \left(\frac{K_{m,\mathrm{O_2}}}{K_{m,\mathrm{O_2}} + [\mathrm{O_2}]} \right)$	E2
$R3 = k_{\alpha,\beta} OM^{\alpha,\beta} \left(\frac{[\mathrm{Mn(OH)_2}]}{K_{m,\mathrm{Mn(OH)_2}} + [\mathrm{Mn(OH)_2}]} \right) \left(\frac{K_{m,\mathrm{NO_3}^-}}{K_{m,\mathrm{NO_3}^-} + [\mathrm{NO_3}^-]} \right) \left(\frac{K_{m,\mathrm{O_2}}}{K_{m,\mathrm{O_2}} + [\mathrm{O_2}]} \right)$	E3
$R4 = k_{\alpha,\beta} OM^{\alpha,\beta} \left(\frac{[\mathrm{Fe(OH)_3}]}{K_{m,\mathrm{Fe(OH)_3}} + [\mathrm{Fe(OH)_3}]} \right) \left(\frac{K_{m,\mathrm{Mn(OH)_2}}}{K_{m,\mathrm{Mn(OH)_2}} + [\mathrm{Mn(OH)_2}]} \right) \left(\frac{K_{m,\mathrm{NO_3}^-}}{K_{m,\mathrm{NO_3}^-} + [\mathrm{NO_3}^-]} \right) \left(\frac{K_{m,\mathrm{O_2}}}{K_{m,\mathrm{O_2}} + [\mathrm{O_2}]} \right)$	E4
$R5 = k_{\alpha,\beta} OM^{\alpha,\beta} \left(\frac{[\mathrm{SO_4}^{2-}]}{K_{m,\mathrm{SO_4}^{2-}} + [\mathrm{SO_4}^{2-}]} \right) \left(\frac{K_{m,\mathrm{Fe(OH)_3}}}{K_{m,\mathrm{Fe(OH)_3}} + [\mathrm{Fe(OH)_3}]} \right) \left(\frac{K_{m,\mathrm{Mn(OH)_2}}}{K_{m,\mathrm{Mn(OH)_2}} + [\mathrm{Mn(OH)_2}]} \right) \left(\frac{K_{m,\mathrm{NO_3}^-}}{K_{m,\mathrm{NO_3}^-} + [\mathrm{NO_3}^-]} \right) \left(\frac{K_{m,\mathrm{O_2}}}{K_{m,\mathrm{O_2}} + [\mathrm{O_2}]} \right)$	E5
$R6 = k_{\alpha,\beta} OM^{\alpha,\beta} \left(\frac{K_{m,\mathrm{SO_4}^{2-}}}{K_{m,\mathrm{SO_4}^{2-}} + [\mathrm{SO_4}^{2-}]} \right) \left(\frac{K_{m,\mathrm{Fe(OH)_3}}}{K_{m,\mathrm{Fe(OH)_3}} + [\mathrm{Fe(OH)_3}]} \right) \left(\frac{K_{m,\mathrm{Mn(OH)_2}}}{K_{m,\mathrm{Mn(OH)_2}} + [\mathrm{Mn(OH)_2}]} \right) \left(\frac{K_{m,\mathrm{NO_3}^-}}{K_{m,\mathrm{NO_3}^-} + [\mathrm{NO_3}^-]} \right) \left(\frac{K_{m,\mathrm{O_2}}}{K_{m,\mathrm{O_2}} + [\mathrm{O_2}]} \right)$	E6
$R7 = k_1 DIC \left(\frac{K_{m,\mathrm{SO_4}^{2-}}}{K_{m,\mathrm{SO_4}^{2-}} + [\mathrm{SO_4}^{2-}]} \right) \left(\frac{K_{m,\mathrm{Fe(OH)_3}}}{K_{m,\mathrm{Fe(OH)_3}} + [\mathrm{Fe(OH)_3}]} \right) \left(\frac{K_{m,\mathrm{Mn(OH)_2}}}{K_{m,\mathrm{Mn(OH)_2}} + [\mathrm{Mn(OH)_2}]} \right) \left(\frac{K_{m,\mathrm{NO_3}^-}}{K_{m,\mathrm{NO_3}^-} + [\mathrm{NO_3}^-]} \right) \left(\frac{K_{m,\mathrm{O_2}}}{K_{m,\mathrm{O_2}} + [\mathrm{O_2}]} \right)$	E7
Secondary redox and other reaction equations	
$R8 = k_2 [\mathrm{O_2}][\mathrm{NH_4}^+]$	E8
$R9 = k_3 [\mathrm{O_2}][\mathrm{Fe}^{2+}]$	E9
$R10 = k_4 [\mathrm{O_2}][\mathrm{FeS}]$	E10
$R11 = k_5 [\mathrm{O_2}][\mathrm{FeS_2}]$	E11
$R12 = k_6 [\mathrm{O_2}][\sum \mathrm{H_2S}]$	E12
$R13 = k_7 [\mathrm{O_2}][\mathrm{CH_4}]$	E13
R14 = $k_8 [\mathrm{Fe(OH)_3}^{\alpha}][\sum \mathrm{H_2S}]$	E14
R15 = $k_9 [\mathrm{Fe(OH)_3}^{\beta,\beta(max),\beta(pulse)}][\sum \mathrm{H_2S}]$	E15
$R16 = k_{10} [\mathrm{Fe}^{2+}][\sum \mathrm{H_2S}]$	E16
$R17 = k_{11} [\mathrm{FeS}][\sum \mathrm{H_2S}]$	E17
$R18 = k_{12} [\mathrm{S}^0]$	E18
$R19 = k_{13} [\mathrm{Fe}^{2+}][\mathrm{S}^0]$	E19
$R20 = k_{14} [\mathrm{SO_4}^{2-}][\mathrm{CH_4}]$	E20
R21 = $k_{15} [\mathrm{Fe(OH)_3}^{\alpha,\beta,\beta(max),\beta(pulse)}][CH_4]$	E21
R22 = $k_{16} [\mathrm{Fe(OH)_3}^{\alpha}]$	E22
$R23 = k_{17} [\mathrm{Fe}^{2+}][\mathrm{HCO_3}^-]$	E23
$R24 = k_{18} [\mathrm{Fe_3(HPO_4}^{2-})_2][\sum \mathrm{H_2S}]$	E24
$R25 = k_{19} [\mathrm{Mn}^{2+}][\mathrm{HCO_3}^-]$	E25
$R26 = k_{20} [\mathrm{Mn}^{2+}][\mathrm{O_2}]$	E26
R27 = $k_{21} [\mathrm{Mn(OH)_2}^{\alpha,\beta}][\mathrm{HPO_4^{2-}}][\mathrm{Fe}^{2+}]$	E27
$R28 = k_{22} [\mathrm{Mn(OH)_2}^{\alpha}][\sum \mathrm{H_2S}]$	E28
R29 = $k_{23} [\mathrm{Mn(OH)_2}^{\beta}][\sum \mathrm{H_2S}]$	E29
R30 = $k_{24} [\mathrm{Mn(OH)_2}^{\alpha}]$	E30
R31 = $k_{25} [\mathrm{Mn(OH)_2}^{\alpha,\beta}][CH_4]$	E31
R32 = $k_{26} [\mathrm{Fe(OH)_3}^{\beta,\beta(max),\beta(pulse)}][\mathrm{HPO_4^{2-}}]$	E32

Table S.7. Reaction parameters used in the model.

Parameter	Value	Unit	Source	Values in literature
k_α	0.3	yr^{-1}	a,b	0.05-1.62
k_β	0.0086	yr^{-1}	b,h	0.0025-0.0086
K_{O_2}	20	$\mu m\ L^{-1}$	c	1-30
$K_{NO_3^-}$	4	$\mu m\ L^{-1}$	c	4-80
$K_{Mn(OH)_2}$	4	$\mu m\ g^{-1}$	c	4-32
$K_{Fe(OH)_3}$	65	$\mu m\ g^{-1}$	c	65-100
$K_{SO_4^{2-}}$	1.6	$\mu m\ L^{-1}$	c	1.6
k1 (E7)	0.044	yr^{-1}	i	0.0011
k2 (E8)	10000	mmol yr^{-1}	c,d	5000-39000
k3 (E9)	$1.4*10^5$	mmol yr^{-1}	c	$1.4*10^5$
k4 (E10)	300	mmol yr^{-1}	c	300
k5 (E11)	1	mmol yr^{-1}	c	1
k6 (E12)	160	mmol yr^{-1}	c	160
k7 (E13)	10^7	mmol yr^{-1}	c	10^7
k8 (E14)	55	mmol yr^{-1}	c,g,i	8-100
k9 (E15)	44	mmol yr^{-1}	c,j	0.004-100
k10 (E16)	9000	mmol yr^{-1}	b,d	100-14800
k11 (E17)	10^{-15}	mmol yr^{-1}	e,i	0.0003-3.15
k12 (E18)	3	yr^{-1}	f	3
k13 (E19)	0.0025	mmol yr^{-1}	f,g	0.001-7
k14 (E20)	17	mmol yr^{-1}	c,g	10(c)-120(g)
k15 (E21)	0.0021	mmol yr^{-1}	g,i	$1.6*10^{-7}$ - 0.0074
k17 (E23)	0	mmol yr^{-1}	i	0.0027
k18 (E24)	$8*10^{-4}$	mmol yr^{-1}	i	$8*10^{-4}$
k19 (E25)	0.265	mmol yr^{-1}		Model constrained
k20 (E26)	1200	mmol yr^{-1}	c	800-20.000
k21 (E27)	0.002	mmol yr^{-1}	f	2
k22 (E28)	0.5	mmol yr^{-1}	c	<100.000 (20)
k23 (E29)	0.4	mmol yr^{-1}	c	<100.000 (20)
k24 (E30)	1.8	yr^{-1}	f	1.8
k25 (E31)	0.0017	mmol yr^{-1}		Model constrained
k26 (E32)	3	mmol yr^{-1}		Model constrained
Vmax	10^{-6}	yr^{-1}		Model constrained
half saturation conc. Fe^{2+}	1000	$\mu mol\ yr^{-1}$		Model constrained
half saturation conc. HPO_4^{2-}	1000	$\mu mol\ yr^{-1}$		Model constrained

Sources:[a](Moodley et al., 2005); [b](Reed et al., 2011b); [c](Wang and Van Cappellen, 1996); [d](Reed et al., 2011a); [e](Rickard and Luther, 1997); [f](Berg et al., 2003); [g](Rooze et al., 2016); [h](Reed et al., 2016); [i](Egger et al., 2016a); [j](Egger et al., 2016b);

References

Berg, P., Rysgaard, S., and Thamdrup, B.: Dynamic modeling of early diagenesis and nutrient cycling. A case study in an Arctic marine sediment, American Journal of Science, 303, 905–955, https://doi.org/10.2475/ajs.303.10.905, 2003.

Boudreau, B. P.: A method-of-lines code for carbon and nutrient diagenesis in aquatic sediments, Computers and Geosciences, 22, 479–496, https://doi.org/10.1016/0098-3004(95)00115-8, 1996a.

Boudreau, B. P.: The diffusive tortuosity of fine-grained unlithified sediments, https://doi.org/10.1016/0016-7037(96)00158-5, 1996b.

Boudreau, B. P.: Diagenetic models and their implementation. Modelling transport and reactions in aquatic sediments, vol. 171, https://doi.org/0.I007/97S-3-642-60421-S, 1997.

Egger, M., Kraal, P., Jilbert, T., Sulu-Gambari, F., Sapart, C. J., Röckmann, T., and Slomp, C. P.: Anaerobic oxidation of methane alters sediment records of sulfur, iron and phosphorus in the Black Sea, Biogeosciences, 13, 5333–5355, https://doi.org/10.5194/bg-13-5333-2016, 2016a.

Egger, M., Lenstra, W., Jong, D., Meysman, F. J., Sapart, C. J., Van Der Veen, C., Röckmann, T., Gonzalez, S., and Slomp, C. P.: Rapid sediment accumulation results in high methane effluxes from coastal sediments, PLoS ONE, 11, https://doi.org/10.1371/journal.pone.0161609, 2016b.

Froelich, P. N., Klinkhammer, G. P., Bender, M. L., Luedtke, N. A., Heath, G. R., Cullen, D., Dauphin, P., Hammond, D., Hartman, B., and Maynard, V.: Early oxidation of organic matter in pelagic sediments of the eastern equatorial Atlantic: suboxic diagenesis, Geochimica et Cosmochimica Acta, 43, 1075–1090, https://doi.org/10.1016/0016-7037(79)90095-4, 1979.

Meysman, F. J. R., Boudreau, B. P., and Middelburg, J. J.: Modeling reactive transport in sediments subject to bioturbation and compaction, Geochimica et Cosmochimica Acta, 69, 3601–3617, https://doi.org/10.1016/j.gca.2005.01.004, 2005.

Moodley, L., Middelburg, J. J., Herman, P. M. J., Soetaert, K., and de Lange, G. J.: Oxygenation and organic-matter preservation in marine sediments: Direct experimental evidence from ancient organic carbon-rich deposits, Geology, 33, 889–892, https://doi.org/10.1130/G21731.1, 2005.

Petzold, L.: Automatic selection of methods for solving stiff and nonstiff systems of ordinary differential equations, SIAM J Sci and Stat Comput, 4, 136–148, https://doi.org/10.1137/0904010, 1983.

Redfield, A. C.: The Biological Control of Chemical Factors in the Environment, American Scientist, 46, 205–221, https://doi.org/10.2307/27828530, http://www.jstor.org/stable/27827150, 1958.

Reed, D. C., Slomp, C. P., and de Lange, G. J.: A quantitative reconstruction of organic matter and nutrient diagenesis in Mediterranean Sea sediments over the Holocene, Geochimica et Cosmochimica Acta, 75, 5540–5558, https://doi.org/10.1016/j.gca.2011.07.002, http://dx.doi.org/10.1016/j.gca.2011.07.002, 2011a.

Reed, D. C., Slomp, C. P., and Gustafsson, B. G.: Sedimentary phosphorus dynamics and the evolution of bottom-water hypoxia: A coupled benthic-pelagic model of a coastal system, Limnology and Oceanography, 56, 1075–1092, https://doi.org/10.4319/lo.2011.56.3.1075, 2011b.

Reed, D. C., Gustafsson, B. G., and Slomp, C. P.: Shelf-to-basin iron shuttling enhances vivianite formation in deep Baltic Sea sediments, Earth and Planetary Science Letters, 434, 241–251, https://doi.org/10.1016/j.epsl.2015.11.033, http://dx.doi.org/10.1016/j.epsl.2015.11.033, 2016.

Rickard, D. and Luther, G. W.: Kinetics of pyrite formation by the H2S oxidation of iron (II) monosulfide in aqueous solutions between 25 and 125C: The mechanism, Geochimica et Cosmochimica Acta, 61, 135–147, https://doi.org/10.1016/S0016-7037(96)00322-5, 1997.

Rooze, J., Egger, M., Tsandev, I., and Slomp, C. P.: Iron-dependent anaerobic oxidation of methane in coastal surface sediments: Potential controls and impact, Limnology and Oceanography, https://doi.org/10.1002/lno.10275, 2016.

Soetaert, K. and Meysman, F.: Reactive transport in aquatic ecosystems: Rapid model prototyping in the open source software R, Environmental Modelling and Software, 32, 49–60, https://doi.org/10.1016/j.envsoft.2011.08.011, http://dx.doi.org/10.1016/j.envsoft.2011.08.011, 2012.

Soetaert, K., Petzoldt, T., and Meysman, F. J. R.: Marelac: Tools for Aquatic Sciences v2.1.3, R package, 2010.

Van Cappellen, P. and Wang, Y.: Cycling of iron and manganese in surface sediments: A general theory for the coupled transport and reaction of carbon, oxygen, nitrogen, sulfur, iron, and manganese, American Journal of Science, https://doi.org/10.2475/ajs.296.3.197, 1996.

Wang, Y. F. and Van Cappellen, P.: A multicomponent reactive transport model of early diagenesis: Application to redox cycling in coastal marine sediments, Geochimica Et Cosmochimica Acta, 60, 2993–3014, https://doi.org/10.1016/0016-7037(96)00140-8, 1996.